Title

Sympathetic modulation of electrical activation in normal and infarcted myocardium: implications for arrhythmogenesis

Journal

AJP Heart and Circulatory Physiology, 312(3)

ISSN

0363-6135

Authors

Ajijola, Olujimi A
Lux, Robert L
Khahera, Anadjeet
et al.

Publication Date

2017-03-01

DOI

10.1152/ajpheart.00575.2016

Peer reviewed

Am J Physiol Heart Circ Physiol 312: H608–H621, 2017.
First published January 13, 2017; doi:10.1152/ajpheart.00575.2016.

RESEARCH ARTICLE | *Cardiovascular Neurohormonal Regulation*

Sympathetic modulation of electrical activation in normal and infarcted myocardium: implications for arrhythmogenesis

Olujimi A. Ajijola,[1,2] Robert L. Lux,[5] Anadjeet Khahera,[1] OhJin Kwon,[1] Eric Aliotta,[3] Daniel B. Ennis,[3] Michael C. Fishbein,[4] Jeffrey L. Ardell,[1,2] and Kalyanam Shivkumar[1,2]

[1]*Cardiac Arrhythmia Center, University of California, Los Angeles, California;* [2]*Neurocardiology Research Center of Excellence, University of California, Los Angeles, California;* [3]*Department of Radiology, University of California, Los Angeles, California;* [4]*Department of Pathology, University of California, Los Angeles, California; and* [5]*Cardiovascular Research and Training Institute, University of Utah, Salt Lake City, Utah*

Submitted 22 August 2016; accepted in final form 4 January 2017

Ajijola OA, Lux RL, Khahera A, Kwon O, Aliotta E, Ennis DB, Fishbein MC, Ardell JL, Shivkumar K. Sympathetic modulation of electrical activation in normal and infarcted myocardium: implications for arrhythmogenesis. *Am J Physiol Heart Circ Physiol* 312: H608–H621, 2017. First published January 13, 2017; doi:10.1152/ajpheart.00575.2016.—The influence of cardiac sympathetic innervation on electrical activation in normal and chronically infarcted ventricular myocardium is not understood. Yorkshire pigs with normal hearts (NL, $n = 12$) or anterior myocardial infarction (MI, $n = 9$) underwent high-resolution mapping of the anteroapical left ventricle at baseline and during left and right stellate ganglion stimulation (LSGS and RSGS, respectively). Conduction velocity (CV), activation times (ATs), and directionality of propagation were measured. Myocardial fiber orientation was determined using diffusion tensor imaging and histology. Longitudinal CV (CV_L) was increased by RSGS (0.98 ± 0.11 vs. 1.2 ± 0.14m/s, $P < 0.001$) but not transverse CV (CV_T). This increase was abrogated by β-adrenergic receptor and gap junction (GJ) blockade. Neither CV_L nor CV_T was increased by LSGS. In the peri-infarct region, both RSGS and LSGS shortened ARIs in sinus rhythm (423 ± 37 vs. 322 ± 30 ms, $P < 0.001$, and 423 ± 36 vs. 398 ± 36 ms, $P = 0.035$, respectively) and altered activation patterns in all animals. CV, as estimated by mean ATs, increased in a directionally dependent manner by RSGS (14.6 ± 1.2 vs. 17.3 ± 1.6 ms, $P = 0.015$), associated with GJ lateralization. RSGS and LSGS inhomogeneously modulated AT and induced relative or absolute functional activation delay in parts of the mapped regions in 75 and 67%, respectively, in MI animals, and in 0 and 15%, respectively, in control animals ($P < 0.001$ for both). In conclusion, sympathoexcitation increases CV in normal myocardium and modulates activation propagation in peri-infarcted ventricular myocardium. These data demonstrate functional control of arrhythmogenic peri-infarct substrates by sympathetic nerves and in part explain the temporal nature of arrhythmogenesis.

NEW & NOTEWORTHY This study demonstrates regional control of conduction velocity in normal hearts by sympathetic nerves. In infarcted hearts, however, not only is modulation of propagation heterogeneous, some regions showed paradoxical conduction slowing. Sympathoexcitation altered propagation in all infarcted hearts studied, and we describe the temporal arrhythmogenic potential of these findings.

Listen to this article's corresponding podcast at http://ajpheart.podbean.com/e/sympathetic-nerves-and-cardiac-propagation/.

Address for reprint requests and other correspondence: O. A. Ajijola, UCLA Cardiac Arrhythmia Ctr., UCLA Neurocardiology Research Ctr., David Geffen School of Medicine at UCLA, Ste. 660, Westwood Blvd., Los Angeles, CA 90095-1679 (e-mail: oajijola@mednet.ucla.edu).

autonomic nervous system; sympathetic nerves; conduction velocity; electrical propagation; ventricular arrhythmias

THE AUTONOMIC NERVOUS SYSTEM (ANS) influences cardiovascular physiology and is strongly linked to ventricular arrhythmias (VAs) and sudden cardiac death (SCD) (62). Mechanistically, sympathetic innervation increases repolarization lability and heterogeneity (42, 57) and is associated with arrhythmogenesis (56). Following cardiac injury, there is also extensive structural and functional neural remodeling throughout the cardiac neural hierarchy (1, 18, 41) and it is associated with increased sympathetic tone. In the heart, nerve sprouts have been identified in peri-infarct zones and associated with VAs, via poorly understood mechanisms (9).

Sympathetic innervation, while it directly affects action potential duration (APD) in ventricular tissue (59), has not been shown to directly modulate muscle-to-muscle conduction velocity (CV) and propagation patterns in normal hearts. A prior study found no significant influence of sympathoexcitation on CV or propagation patterns (59). However, the preparation used was limited by a mismatch between the ganglion stimulated and region mapped. Electrical activity was recorded in the region innervated by right sympathetic nerves while the left nerves were stimulated.

We sought to examine whether sympathoexcitation significantly increases C7V in normal hearts and in peri-infarct zones of infarcted hearts. We assessed this by right and left stellate ganglion stimulation (RSGS and LSGS, respectively), with high-resolution mapping of the anterior wall of the left ventricle (LV) in a porcine model with an intact ANS, under anesthetic conditions known to preserve autonomic neural activity and reflexes.

METHODS

Animal subjects. Experimental procedures involving animal subjects were approved by the animal research council and were performed in accordance with guidelines set by both the University of California Institutional Animal Care and Use Committee and the National Institutes of Health *Guide for the Care and Use of Laboratory Animals*. Yorkshire pigs of either sex (50–70 kg) were used for terminal experiments. Twelve control animals and nine infarcted animals (6–8 wk postinfarct) were studied. The anesthetic regimen for terminal experimentation was sedation with Telazol (8–10 mg/kg im) and dexmedetomidine (0.05–0.2 mg/kg) and intubation, and a

sternotomy was performed with an isoflurane (1–2%) and fentanyl (100 μg) intravenous bolus given once at the beginning of the preparation and intermittently during surgery. Following completion of sternotomy, isoflurane was slowly transitioned to α-chloralose solution (6.25 mg/125 ml; bolus 1 ml/kg; maintenance 25–35 ml/kg titrated to effect). Temperature was maintained at 36–38°C with the use of a heated surgical table and a heated blanket. The sternotomy was also kept covered to minimize cardiac cooling and insensible losses. After the experimental protocol was completed, animals were euthanized by pentobarbital sodium (100 mg/kg). Paralytic agents were not used.

Infarct induction. Antero-apical infarcts were induced percutaneously. Animal subjects (35 ± 4.5 kg, $n = 9$) were sedated with Telazol (8–10 mg/kg im) and fentanyl (50–100 μg iv). To accommodate the weight gain during the postinfarct period (6–8 wk), smaller animals were infarcted. As such, the weights of control and infarcted animals were uniform at terminal study. Following intubation, general endotracheal anesthesia and analgesia were maintained with inhaled isoflurane (1 to 2%) and by boluses of fentanyl (50–100 μg iv), respectively. With an 8-French Amplatz left (AL1) coronary guide catheter, a balloon-tipped coronary angioplasty catheter (FoxCross; Abott Vascular, Temecula, CA) was advanced over a guide wire to the mid-left anterior descending coronary artery. The balloon was inflated to subocclusive pressures, and a 5- to 7.5-ml suspension consisting 80% by volume of polystyrene microspheres (90-μm Polybead; Polysciences, Warrington, PA), and radiopaque contrast was slowly injected over 1 to 2 min through the angioplasty catheter. Transmural myocardial ischemia was confirmed by immediate ST-segment elevation in ECG leads I, II, and V1.

Sympathetic stimulation. LSGS and RSGS were performed with repeated square-wave pulses at a frequency of 4-Hz, 4-ms duration for 30 s. Stimulation amplitude was set at the amplitude at which blood pressure and/or heart rate increased by 10% (generally 1–8 mA). Cardiac sympathetic activation was also confirmed by surface T-wave changes and increases in heart rate and blood pressure as previously described (2). Bipolar electrodes were placed around each stellate ganglion (superior and inferior) for stimulation, with the cathode being superior. Over the course of the entire experimental protocol, hemodynamic responses to LSGS and RSGS were maintained, and the preparations remained intact.

Cardiac electrical mapping. A 64-electrode arrray (8×8 configuration, 2-mm interelectrode spacing) was placed on the antero-apical epicardium of the LV in normal animals and in the same region in the peri-infarct zone of infarcted animals. From these arrays, epicardial electrograms (EGMs) were recorded at baseline and during SGS. Following the surgical preparation, animal subjects were allowed to stabilize for 40 min before experiments were commenced. EGMs were recorded with a customized multiplexer (University of Utah, Salt Lake City, UT) (19, 32). Using a previously described customized program (2) to generate the first derivative of the QRS, and second derivative of the T wave, activation time (AT) was measured as the time interval between the onset of ventricular activation and the minimum dV/dt of the QRS and repolarization time (RT) as the maximum dV/dt of the T wave. The activation recovery interval (ARI), a surrogate for APD (27, 32), was taken as the difference between RT and AT (ARI = RT − AT), as previously described.

Electrical maps depicting AT and ARI measured from all electrodes were projected onto a 2-D geometry using publicly available software Map3D (Scientific Computing and Imaging Institute, University of Utah: http://www.sci.utah.edu/cibc/software/107-map3d.html).

Conduction velocity. Bipolar pacing (2-mm bipole spacing resulting in point stimulation) was performed superficially on the epicardium adjacent to the plaque to avoid breakthrough conduction to the surface. Because of the tachycardia seen during RSGS, pacing was performed at 10% above the maximal heart rate seen during RSGS, ≈120 beats/min. CV was measured as the distance traversed across the multielectrode plaque (in mm), divided by the difference in local activation times between the earliest activation (pacing site), and the earliest activation time at the opposite end of the plaque (in ms), i.e., CV = distance traversed/[$AT_{end} - AT_{pacing\ site}$] (see Fig. 2*D*). Data obtained in mm/ms are expressed as m/s for comparison. CV was averaged from five beats at baseline and at 30 s of SGS; however, propagation maps show a single median beat (*beat 3*).

Diffusion tensor MRI. Fiducial markers were placed on the hearts to indicate the exact location of the plaque as it was removed. Rapidly excised hearts were first rinsed with saline, and all cavities werefilled with a silicone rubber resin (Templet Polyvinylsiloxane; Microsonic, Ambridge, PA) to maintain a near end-diastolic geometry during imaging. The hearts were then placed in a plastic cylindrical container filled with a susceptibility-matched fluid (Fomblin; Solvay Solexis, West Deptford, NJ) and held in place using open-cell foam. 3T (Siemens Prisma, Erlangen, Germany) MRI was then performed with T1 weighted imaging using a three-dimensional (3D) Fast Low Angle Shot (FLASH) sequence ($0.5 \times 0.5 \times 0.5$-mm spatial resolution, scan time: 1.5 h). The images were visualized using a 3D volume rendering in Osirix (Pixmeo, Geneva, Switzerland).

Diffusion tensor MRIs (DTIs) were then acquired using a readout segmented diffusion weighted spin echo sequence (20) with b value = 1,000 s/mm^2 along 30 directions and $1.0 \times 1.0 \times 1.0$ mm spatial resolution with 5–10 signal averages to improve signal-to-noise ratio (scan time: 8–10 h). The DTI acquisition was oriented to the epicardial tangent plane in the region immediately below the plaque electrode using the implanted fiducial markers. Ten slices were acquired parallel to the prescribed epicardial plane and analysis was limited to only the most epicardial layer; hence, the DT-MRI maps represent tissue that is within 1 mm of the epicardial surface. Diffusion tensors were reconstructed from the diffusion weighted images using linear regression and custom Matlab (The Mathworks, Natick, MA) software. Care was taken to identify the fiducial markers at all planes examined. Fiber orientations were determined by calculating the primary eigenvector of the diffusion tensor in each voxel and displayed with a color map. The colors correspond to the orientation of the primary eigenvector ("myofiber" long axis) of the diffusion tensor. The x, y, and z components of the vectors are mapped to red, green, and blue, respectively (i.e., horizontal fibers are predominantly red while vertical vectors are green).

All data points in the region immediately below the plaque electrode are displayed. It is well known that myocardial scar leads to an increase in apparent diffusivity compared with healthy tissue (37, 40) as well as a loss of directionality (i.e., anisotropy). In a map of fiber orientation, this will manifest as seemingly random orientations.

At each voxel, the cosine similarity coefficient, a measure of similarity between adjacent fiber orientations (i.e., voxels), was calculated as the difference between each voxel and the average measure of the nine neighboring voxels. Fiber orientations and maps of fiber organization were plotted in the epicardial tangent plane in the region of the plaque electrode as determined by implanted fiducial markers.

Histology and immunohistochemistry. The region under the multielectrode plaque was excised with very tight margins, placed immediately in 10% phosphate-buffered formalin for 5–7 days, and transferred to 70% ethanol. The epicardial and subepicardial layers were cut parallel to the surface for paraffin embedding. Samples were processed for embedding in cassettes with pieces of foam above and below the specimen to keep the tissue completely flat. Once embedded, the epicardial tissue layer was carefully sectioned away (~50–75 μm) until the myocardium was reached. Four-micrometer thin sections of the myocardium were collected for hematoxyline and eosin (H&E) and trichrome elastic von Giesen (Tri-EVG) staining to examine the scar border-zone region mapped. Sympathetic nerves were identified by immunohistochemistry (IHC) antibodies against tyrosine hydroxylase (cat no. ab112, 1:200 dilution; Abcam, Cambridge, MA) and detected by diaminobenzidine reaction (DAB; Life Technologies, Green Island, NY). Connexin density was examined by antibodies

against Cx-43 (cat. no. C6219, 1:2,000 dilution; Sigma, St Louis, MO) and also detected by DAB reaction. Histologic and IHC slides were digitally scanned and electronically stored for analysis (Scan Scope; Aperio, Vista, CA). Immunohistochemical quantifications were performed by computerized morphometry (TissueStudio; Definiens, Parsippany, NJ).

Statistical analyses. Data are reported as means ± SD unless stated otherwise. Multigroup comparisons were performed using a two-way ANOVA. If using ANOVA P was <0.05, then post hoc comparisons were made using the Tukey-Kramer minimum significant difference test. Paired comparisons were performed with the Wilcoxon signed rank test if data were not normally distributed and with the Student t-test for normally distributed data. Comparisons of control and infarcted animal subjects were performed with the Mann-Whitney test. Repeated tests of independence were performed with the Cochran-Mantel-Haenszel test. For all comparisons, $P < 0.05$ was considered statistically significant. Data were analyzed with JMP Pro 11 (SAS, Raleigh, NC) or Systat 13 (Systat, San Jose, CA).

RESULTS

Sympathoexcitation increases CV in normal ventricular myocardium. The experimental preparation and representative examples of EGMs recorded from the antero-apical LV in sinus rhythm and during RSGS and LSGS are shown in Fig. 1*A*. Hemodynamic responses to RSGS and LSGS in this preparation have been previously reported and were not different between control and infarcted animals (2). Compared with baseline values, RSGS shortened ARIs on the anteroapical LV 11-fold greater than LSGS (16.3 ± 6.5 vs. 1.5 ± 2.9%, $P < 0.001$) in sinus rhythm (mean heart rates at baseline and during RSGS and LSGS were 63.3 ± 7, 81.6 ± 9.4, and 66 ± 8.1 beats/min, respectively, $P < 0.001$ for baseline vs. RSGS and RSGS vs. LSGS, $P > 0.2$ for baseline vs. LSGS), and greater than threefold during ventricular pacing (12.4 ± 4.8 vs. 4.3 ± 2.3%, $P < 0.01$; Fig. 1, *B* and *C*). These data indicate that RSGS provides greater functional innervation of the epicardium mapped than LSGS.

Detailed subepicardial fiber orientation for each animal was determined by DT-MRI and histology, and the orientation of GJs, determined by connexin-43 (Cx-43) staining, was confirmed. On the anterior subepicardium, myocardial fiber orientation was predominantly oriented horizontally (Fig. 2, *A* and *B*), and GJs were principally oriented longitudinally (Fig. 2*B*). As expected, transverse CV (CV_T) was slower than longitudinal CV (CV_L), and this relationship remained unchanged by RSGS and LSGS (Fig. 2, *C* and *D*). CV_L was increased by RSGS (0.98 ± 0.11 vs. 1.2 ± 0.14 m/s, $P < 0.001$) but not LSGS (0.99 ± 0.1 vs. 0.95 ± 0.13 m/s, $P = 0.11$; Figs. 2*D* and 3*A*). The time course of the RSGS effect is shown in Fig. 2*E*. Neither RSGS nor LSGS had an effect on CV_T (0.75 ± 0.06 vs. 0.74 ± 0.06 m/s, $P = 0.86$, and 0.74 ± 0.05 vs. 0.79 ± 0.04 m/s, $P = 0.17$, respectively, for RSGS and LSGS; Figs. 2*C* and 3*B*). The anisotropy ratios (ARs, CV_L/CV_T) at baseline and during RSGS and LSGS were 1.4 ± 0.2, 1.7 ± 0.1, and 1.1 ± 0.1, respectively (ANOVA, $P = 0.05$, $P = 0.035$ for RSGS vs LSGS).

Mean AT, another indicator of the rapidity of propagation in the mapped epicardium, was similarly shorter in the longitudinal direction of propagation, relative to transverse (11.5 ± 0.7 vs. 14.9 ± 1.0 ms, $P < 0.001$; Fig. 3*C*), a relationship unchanged by either SGS (10.4 ± 1.0 vs. 14.6 ± 0.8 ms, $P < 0.001$ for RSGS, and 11.3 ± 0.7 vs. 14.3 ± 1.1 ms, $P = 0.015$

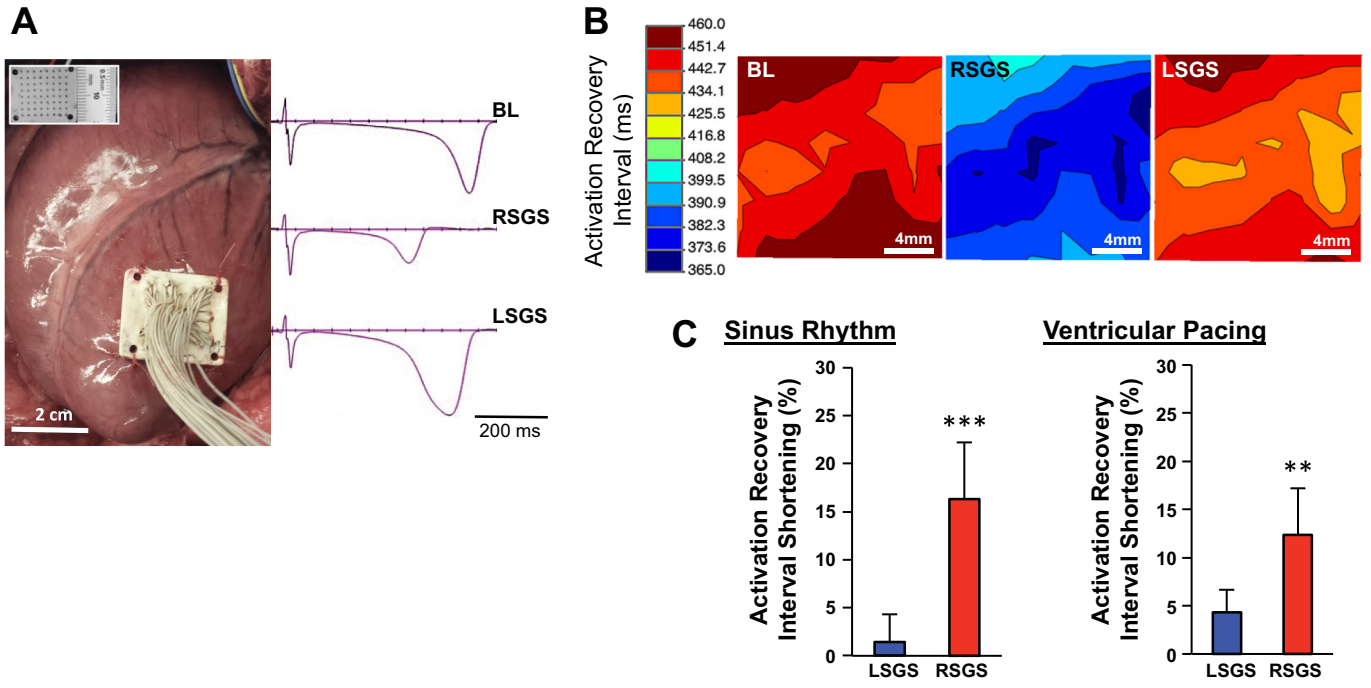

Fig. 1. Influence of left and right sympathetic ganglia on activation recovery intervals in the anterior left ventricle. *A*: experimental preparation is shown, with the location of the left ventricle mapped. The high-density mapping array is shown in the *inset*. Representative examples of electrograms recorded at baseline and during left and right stellate ganglion stimulation (LSGS and RSGS, respectively) are also shown. *B*: representative electrical maps showing of the impact of RSGS and LSGS on activation recovery intervals (ARIs), a surrogate for local action potential duration (APD), are shown. Bl, baseline. *C*: quantifications of the differential effects of LSGS and RSGS on ARIs in sinus rhythm and during ventricular pacing are shown ($n = 8$, $^{**}P < 0.01$, $^{***}P < 0.001$, Wilcoxon signed rank test).

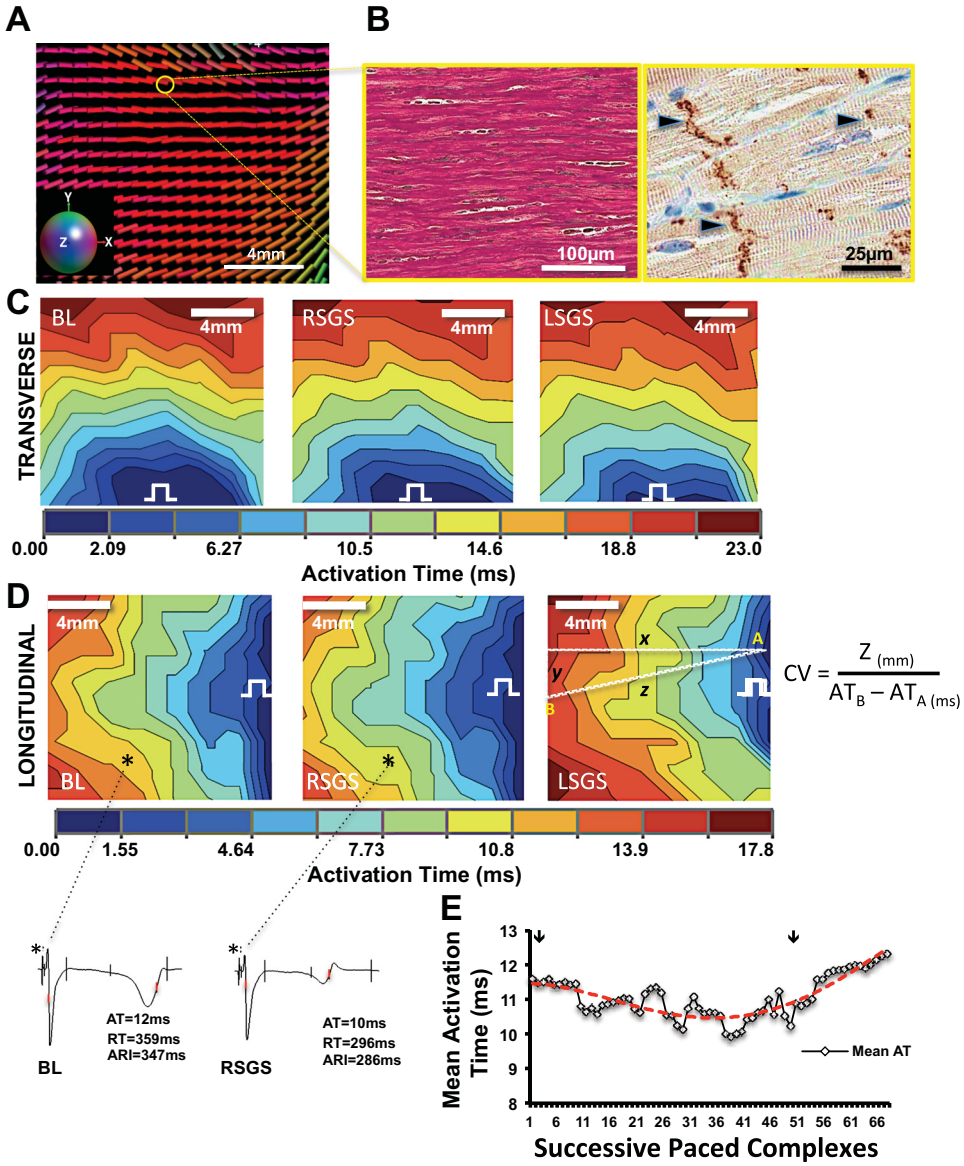

Fig. 2. Sympathoexcitation increases conduction velocity in normal hearts: influence of fiber orientation and gap junction distribution. *A*: representative diffusion tensor magnetic resonance (DT-MRI) image of the region mapped on the left ventricle (LV). The colors correspond to the orientation of the primary eigenvector ("myofiber" long-axis) of the diffusion tensor. The *x*, *y*, and *z* components of the vectors are mapped to red, green and blue, respectively (*inset*). *B*: representative examples of fiber orientation (trichrome elastic Von Giesen stain), and gap junction (GJ) distribution (black arrowheads) shown by connexin-43 immunoreactivity in normal myocardium are shown, respectively. *C*: activation maps showing propagation. transverse and *D*: longitudinal directions at baseline, and during right and left stellate ganglion stimulation (RSGS and LSGS, respectively). Electrical step symbol indicates pacing site. Electrograms from the sites indicated by the asterisks in *D* are also shown. *E*: time course of RSGS on activation propagation (as estimated by activation time) is shown. Arrows indicate the initiation and termination of RSGS.

for LSGS). However, RSGS shortened mean AT ($P = 0.035$) in the longitudinal direction compared with baseline, while LSGS did not ($P = 0.2$). Spatial activation heterogeneity (AT variance per cm^2), a marker of dissimilarity in activation times over the area mapped, was similarly lower with longitudinal than transverse propagation (12.4 ± 1.3 vs. 22.1 ± 1.5 ms^2/cm^2, $P = 0.003$). In these normal hearts, neither RSGS nor LSGS significantly changed spatial activation heterogeneity (Fig. 3*D*).

To ascertain whether increased CV was mediated by β-adrenergic signaling, intravenous esmolol (2.0–2.2 mg/kg) was slowly administered until a >10% drop in heart rate and/or blood pressure were recorded. As shown in Fig. 3*E*, β-blockade eliminated the increase in CV_L seen with RSGS. Given the dependence of RSGS-mediated CV increase on fiber orientation (and hence GJ distribution), we examined whether the increase in CV_L was mediated via GJ modulation. Cellular uncoupling was achieved with carbenoxolone (1.4–1.6 mg/kg), a GJ blocker (14, 26), resulting in complete abrogation of the CV_L response to RSGS 24.7 ± 8.9, −2.6 ± 3.7, and −2.8 ± 3.9% ($P < 0.001$), respectively, for control, esmolol, and carbenoxolone, respectively (Fig. 3, *E* and *F*). Mean CV_L and CV_T following carbenoxolone administration were 0.9 ± 0.1 and 0.62 ± 0.1 m/s.

The impact of RSGS on excitation properties of the myocardium during pacing, as estimated by the magnitude of the maximal negative slope of the local activation complex ($-dV/dt_{max}$) was obtained from local unipolar EGMs (21). As shown in Fig. 3*G*, $-dV/dt_{max}$ values were not different between baseline and RSGS during pacing (−313.3 ± 80.5 vs. −337 ± 80.2 mV/ms, $P = 0.2$).

Influence of SGS on sinus rhythm activation and APD in peri-infarct regions. To examine how SGS modulates activation propagation around infarcts, detailed structural characterization of the peri-infarct zone was performed. As previously reported, the peri-infarct zones are heterogeneous and patchy, with islands of surviving myocardium distributed within dense scar regions (10, 15, 44, 48, 59, 60) (Fig. 4, *A* and *B*). These

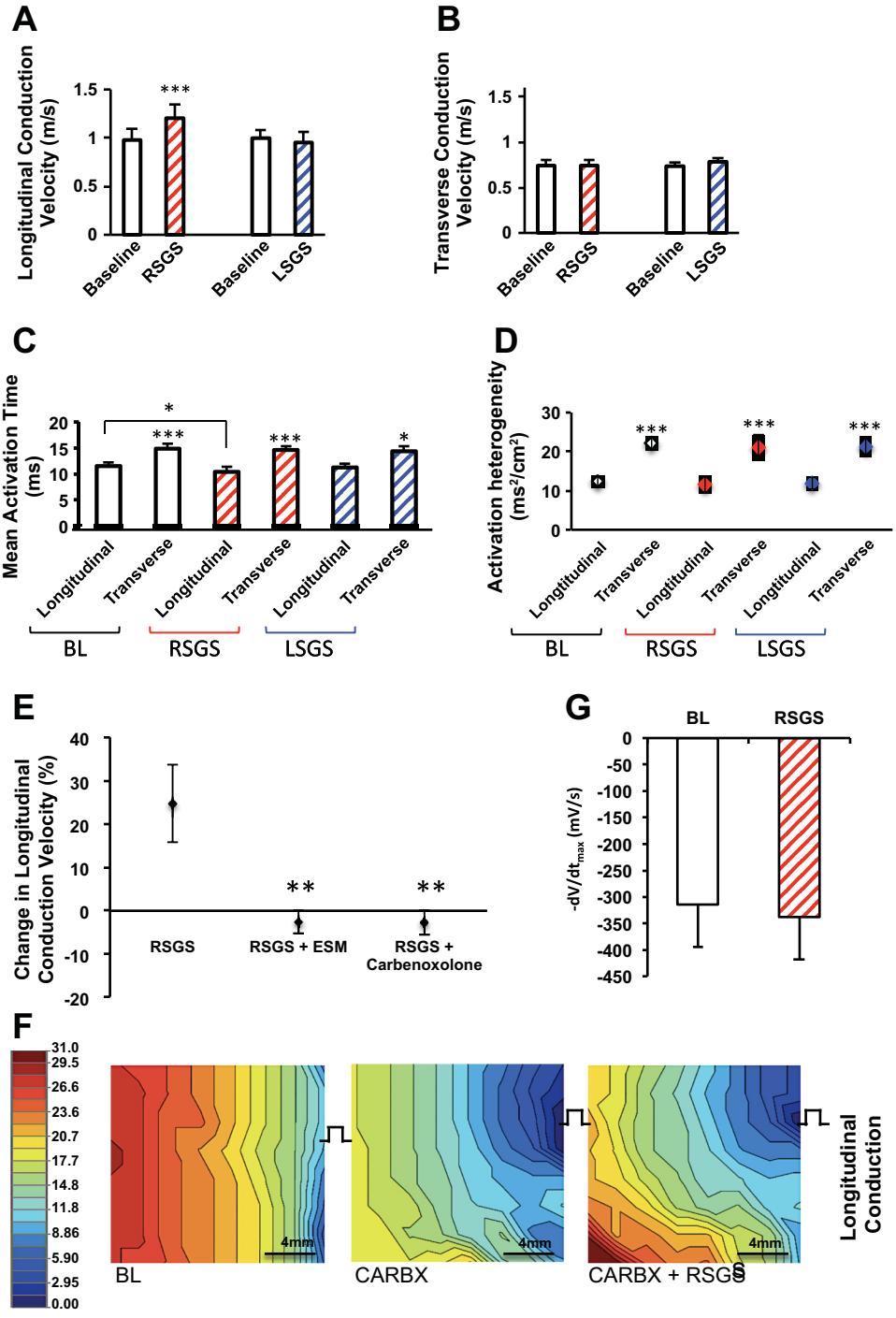

Fig. 3. Sympathoexcitation and conduction velocity in normal hearts. *A–D*: graphs showing the impact of RSGS and LSGS on longitudinal and transverse conduction velocity (CV), mean activation time, and activation heterogeneity ($n = 12$, $^{*}P < 0.05$, $^{***}P < 0.001$, Wilcoxon signed rank test). *E*: graphs showing the impact of esmolol (ESM) and carbenoxolone on change in CV during RSGS ($n = 3$, $^{**}P < 0.01$, Wilcoxon signed rank test). *F*: representative activation maps depicting the effect of carbenoxolone (CARBX) ± RSGS on longitudinal propagation. *G*: maximal negative slope of activation waveform ($-dV/dt_{max}$) of electrograms during pacing at baseline and during RSGS ($n = 5$, $^{**}P = 0.2$, Wilcoxon signed rank test).

peri-infarct zones demonstrate large and small nerve bundles and sprouts positive for tyrosine hydroxylase (TH) (Fig. 4, *C* and *D*). Interestingly, compared with normal pigs in which myocardial fiber orientation on the epicardium is generally arranged horizontally in the anteroapical LV, myofiber orientation in the infarcted heart maintained similar orientation as it approached the edge of the dense infarct (Fig. 4, *C* and *D*). At the scar edges, however, there was considerable anisotropy of peri-infarct fiber orientation (Fig. 4, *E* and *F*).

In the peri-infarct region, there was no significant difference in baseline sinus rhythm ARI between control and MI animals (397 ± 65 vs. 422 ± 94 ms, $P = 0.7$). Both RSGS and LSGS significantly shortened ARI in peri-infarct regions (423 ± 37 vs. 322 ± 30 ms, $P < 0.001$, and 423 ± 36 vs. 398 ± 36 ms, $P = 0.035$, respectively; Fig. 5, *A* and *C*). Unlike control animals where LSGS did not result in ARI shortening in the anteroapical region, LSGS had a significant impact in infarcted animals, although this effect was modest compared with RSGS. Mean heart rates at baseline and during RSGS and

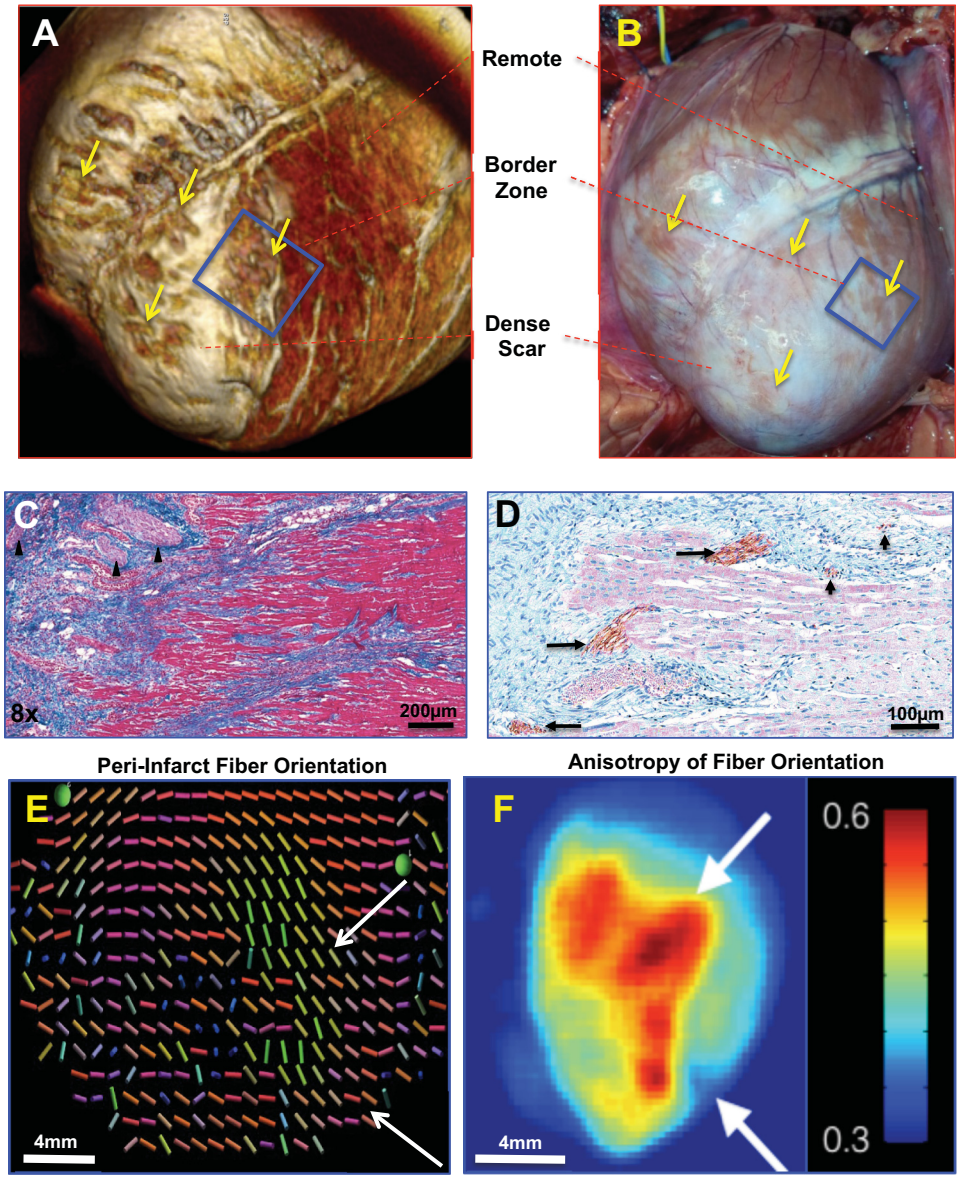

Fig. 4. Characterization of peri-infarct zones. *A*: 3D reconstructed magnetic resonance image of the peri-infarct zone. *B*: photograph of the same heart in *A* before mapping. The box indicates the regions mapped, while the black arrows indicated surviving islands of myocytes in the peri-infarct region. *C*: trichrome elastic Von Giesen stain of the peri-infarct region, with nerve bundles indicated by the arrowhead. The linear arrangement of the surviving myocytes can be easily seen. *D*: tyrosine hydroxylase immunoreactivity highlighting cardiac sympathetic nerves in the scar border is shown. Both large (long arrows) and small (short arrows) nerve bundles can be easily seen. *E*: diffusion tensor magnetic resonance image showing fiber disarray in the peri-infarct zone (the colors of each vector bar represents 3D orientation of the local myofiber). *F*: accompanying heat map to *E*. Scale bar is in arbitrary units of dissimilarity between adjacent fibers as shown in *E*.

LSGS were 68.7 ± 5.6, 98 ± 8, and 73.2 ± 6.1 beats/min, respectively, $P < 0.001$ for baseline vs. RSGS, $P = 0.035$ for RSGS vs LSGS, and $P = 0.2$ for baseline vs. LSGS).

Mean AT of the peri-infarct region was not significantly different in sinus rhythm between control and MI animals (19.6 ± 1.3 vs. 21.7 ± 1.9 ms, $P = 0.2$); however, MI animals demonstrated greater spatial activation heterogeneity compared with the same region in control animals (12.4 ± 4 vs. 4.1 ± 0.6 ms^2/cm^2, $P = 0.044$) in sinus rhythm. RSGS significantly shortened mean AT in the peri-infarct zone (17.6 ± 1.6 vs. 21.0 ± 1.8 ms, $P = 0.035$) in sinus rhythm, while LSGS did not result in significant mean AT shortening (19.7 ± 1.7 vs. 21.8 ± 2.4 ms, $P = 0.2$; Fig. 5, *B* and *D*). An example of a subject in which LSGS shortened mean AT is depicted in Fig. 5*B*. It can also be easily noted that SGS nonuniformly modulated AT and ARI (APD) in the peri-infarct zone.

SGS and inhomogeneous activation propagation in peri-infarct regions. In the peri-infarct zone, the path taken by activation wavefront may not always be captured by the array; therefore, changes in AT in the mapped area were used to approximate the rapidity of propagation. Furthermore, due to the loss of tissue architecture, and the presence of scar in the mapped area, longitudinal and transverse fiber orientations do not accurately describe propagation patterns. Therefore, to determine the impact of SGS on CV, we examined two pacing wavefronts in the peri-infarct zone as depicted in Fig. 6*A*. Wavefronts I and II are directed along and toward the dense scar border in MI.

Compared with baseline, RSGS but not LSGS significantly decreased mean AT in the peri-infarct zone (17.3 ± 1.6 vs. 14.6 ± 1.2 ms, $P = 0.015$, and 15.5 ± 1.0 ms, $P = 0.075$, respectively). Interestingly, this decrease was seen only for wavefront I but not II (Fig. 6, *B* and *C*). More importantly, regardless of the effect on mean AT, RSGS and LSGS inhomogeneously altered AT, frequently exposing relative (i.e., compared with adjacent regions after SGS) or absolute (compared with the same site at baseline) delay in activation in the peri-infarct zone (Fig. 6*B*, asterisk). Furthermore, in all animals studied, the pattern of electrical activation was changed by

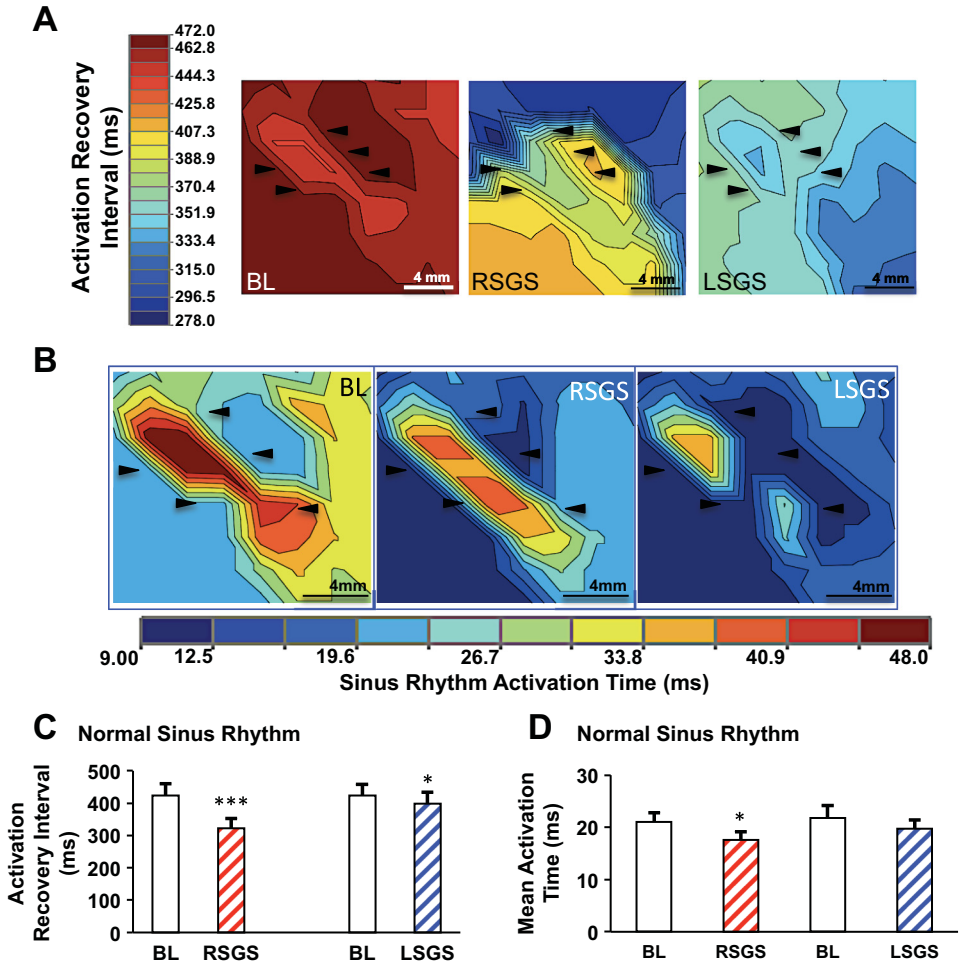

Fig. 5. Sympathetic nerves exert functional control of sinus rhythm activation and repolarization in the peri-infarct zone. Maps depicting a peri-infarct zone and the influence of right and left stellate ganglion stimulation (RSGS and LSGS), respectively, on activation recovery intervals (ARIs), a surrogate for action potential duration (*A*), and activation in sinus rhythm (*B*); black arrows in *A* and *B* highlight the same region for comparison across conditions. Heart rate (HR) for each map is shown in the top right corner of *A*; bpm/beats/min. Composite data is shown in *C* and *D*. for ARI and mean activation time ($n = 7$, $^{***}P < 0.001$, $^{*}P < 0.05$, Wilcoxon signed rank test).

RSGS and/or LSGS. In control animals, spatially homogeneous changes in activation were induced by SGS. In the peri-infarct zone, ATs were unchanged, shortened, or paradoxically increased during SGS (Fig. 6, *B* and *D*). As shown in Fig. 6*E*, these spatial differences in activation were seen in 75 and 67% of RSGS and LSGS maps, respectively, in MI animals, and in 0 and 15% respectively in control animals ($P < 0.001$ for both RSGS and LSGS).

To examine whether GJ distribution was related to the direction influence of RSGS on propagation, we examined the distribution of Cx-43 immunoreactivity in peri-infarct zones mapped. As shown in Fig. 6, *F–H*, compared with the longitudinal distribution of Cx-43 in control hearts, there was greater than a threefold ($P < 0.001$) increase in GJ lateralization in the peri-infarct zone, along with decreased density (2.8-fold, $P = 0.03$). Interestingly, this lateralized location was consistent with the direction of propagation of wavefront I, suggesting that these lateralized GJs were influenced by RSGS. Spatial heterogeneity of activation (Fig. 6*I*) for wavefronts I and II at baseline was 20.7 ± 5.1 and 13.1 ± 2 ms^2/cm^2 ($P = 0.075$). During RSGS, these values were 14 ± 4.1 and 15.7 ± 4 ms^2/cm^2, respectively, and during LSGS, 15.1 ± 4.4 and 19.1 ± 7 ms^2/cm^2, respectively ($P > 0.2$ when compared with baseline and between SGS types). In sinus rhythm, activation heterogeneity at baseline and during RSGS and LSGS was 11.7 ± 3.7, 10.4 ± 4.5, and 10.7 ± 3.1 ms^2/cm^2.

SGS can alter propagation in putative ventricular tachycardia circuits. In diseased myocardium, late potentials and local abnormal ventricular activations are seen after or within the QRS, respectively, and reflect regions with delayed or abnormal electrical propagation. Often, ventricular arrhythmias are induced by unidirectional block in such regions, and these sites become critical isthmuses for monomorphic ventricular tachycardia (MMVT). An example of a late potential and the impact of SGS on propagation is shown in Fig. 7*A*. Two adjacent electrodes (E1 and E9) mapping electrical activity in the upper left corner of the array are displayed. During SGS, conduction through this region exhibited alternating functional block (2:1 propagation). Mean AT in the region mapped was longer when the late potential was present than when absent (9.3 ± 2.7 vs. 8.6 ± 2.8 ms, $P < 0.001$), indicating conduction block into that region or more rapid propagation such that the LP is no longer present (Fig. 7, *B* and *C*, respectively). Local ARIs recorded in the focal region (0.12 cm^2) demonstrating alternating conduction were not significantly different between beats with and without the late potential (291.7 ± 1.3 vs. 293.7 ± 3.0 ms, $P = 0.2$).

DISCUSSION

The major findings of the present study are *1*) CV_L is increased directly by excitation of sympathetic fibers inner-

vating the ventricles, mediated partly by GJ conductance; *2*) in peri-infarct zones, characterized by extensive connexin lateralization, rapidity of activation propagation is increased by sympathoexcitation parallel to the scar border in the apico-basal axis; *3*) sympathoexcitation induces inhomogeneous changes on activation and even paradoxically prolongs activation propagation at some peri-infarct sites; and *4*) peri-infarct propagation in putative VT circuits can be altered by SGS. This represents the first demonstration of these electrophysiologic phenomena by direct cardiac sympathetic innervation, in an experimental preparation with intact cardiac neuraxial control, mapped in vivo, under an anesthetic regimen that does not suppress autonomic function.

The CVs obtained in normal animals in our study are in line with prior examinations of CV in various preparations (6). Although the CVs we report are at the higher end of the spectrum, they are within accepted values (10, 15, 44, 48, 60). The ARs in this study (≈1.4) are also lower than prior studies (range 2–10) (10, 15, 44). The somewhat higher CV values and lower ARs are likely due to the differences in experimental preparations, which include myocardial strips in a bath (10), low temperature (36, 59), and a decentralized preparation (50). Furthermore, compared with the intact beating heart in vivo, factors critical to CV such as cell geometry and size, connexin turnover and GJ distribution, and cellular excitability are not completely maintained in myocardial strips or Langendorff-perfused hearts (46). Although pacing from the center of the array may have yielded different CV and AR values, other studies with different pacing wavefronts similar to this study had higher AR values (10, 15, 44). Differences may also be related to species, as differences in CVs have been reported across species (15). While Purkinje fibers in the pig are known to exist transmurally in the porcine ventricle (4) unlike some other species (50), it is unlikely that Purkinje conduction contributed to these values, due to its orientation in the ventricular wall (15) and CV values that are well below the 2–3 m/s range recorded for Purkinje conduction (11).

Modulation of propagation in normal hearts by sympathoexcitation. The characterization of cardiac electrical responses to sympathoexcitation has largely been limited to repolarization dynamics (38). The effects of sympathetic excitation include APD shortening via modulation of the slow inward rectifying potassium channel (IK_S), increased repolarization heterogeneity, increased intracellular calcium, and increased afterdepolarizations (5), among other effects. The sodium channel NaV1.4 (encoded by *SCN5A*) is known to be upregulated and modulated by β-adrenergic stimulation (13, 31). However, this is on a longer time scale and unlikely to have played a role on the short-term effects of SGS studied here. On short time scales, β-adrenergic stimulation was shown in single cell experiments to increase the sodium current by recruiting sodium channels to the membrane (29). GJs, which can be regulated via a variety of mechanisms, represent a dynamic target of β-adrenergic receptor activation (7). This can occur via accumulation of GJs at the intercalated disks, increased GJ expression, and increased permeability or conductance (17), although controversy exists over this latter mechanism (43), occurring via cyclic AMP (cAMP)-protein kinase A (PKA)-mediated phosphorylation of Cx43. There is substantial evidence from in vitro preparations that GJ function can be modulated by β-adrenergic receptor (BAR) activation on short and long times scales (7). Whether the velocity of muscle-to-muscle propagation directly under the influence of cardiac sympathetic nerves is increased and what are the mechanisms underlying such increases remain unknown.

Wallace and Sarnoff (59) examined the effects of sympathetic nerve stimulation on ventricular conduction. In their studies, sympathetic nerve stimulation (SNS) was accomplished by LSGS, and the anterior aspect of the LV was mapped. The authors observed that sympathoexcitation by LSGS had no significant impact on myocardial CV, and in fact, some sites showed an increase in AT. These experiments were, however, limited by discordance of the ganglion stimulated and the region mapped, the decentralization of the LSG, and in some cases the complete removal of the RSG. Using electrophysiologic indexes to examine the functional innervation patterns of left and right sympathetic nerves on the heart, our group and others have demonstrated that the anterior wall of the heart is innervated predominantly by the RSG, while the posterior wall is innervated by the LSG (2, 53, 63). Cardiac sympathetic denervation is frequently performed for intractable arrhythmias, however, left cardiac sympathectomy is still widely performed. One implication of the present study is that unilateral (left-sided) sympathectomy may be inadequate for arrhythmia control if the VT originates from the anterior wall. This may account for certain failures of left sympathectomy for arrhythmia control and emphasizes the role of bilateral sympathetctomy over unilateral (55).

In the present study, the anterior LV was mapped during RSGS, in a nondecentralized preparation (intact nerve connections), under an anesthetic regimen in which autonomic nerve activity and reflexes were maintained. We confirmed greater functional innervation of the mapped region by RSGS than LSGS and demonstrated increased CV_L but not CV_T during sympathoexcitation. With the use of DT-MRI and histology, our findings on subepicardial myofiber orientation patterns are consistent with Streeter et and Bassett (52), who similarly examined this in porcine. We further demonstrated that the differential effect of RSGS on CV_L vs. CV_T was mediated by the distribution of GJs, known to exist predominantly at end-to-end intercalated disks than side-to-side in normal hearts, by inducing cellular uncoupling (14, 26). This eliminated the increase in CV_L during RSGS. A number of factors may account for the increase in CV_L but not CV_T. The relationship between CV and GJ conductance is not linear and differs for CV_L and CV_T. For a specific GJ conductance, intercellular resistivity, a major determinant of CV, is greater in the transverse than longitudinal direction, related to size of GJ plaques and connexin density (22). Equal modulation of GJ conductance may therefore yield different degrees of change in CV.

Furthermore, while the effects of β-adrenergic activation are myriad, how the relationships among GJ conductance, intercellular resistivity, and CV change following adrenergic stimulation is not well understood but may differ for CV_T and CV_L. Another important factor is the differential impact of steady-state pacing frequencies on CV_L and CV_T. Spach et al. (49) examined the CV at increasing steady-state pacing frequencies and found that CV_T decreased to a greater extent than CV_L. It is entirely possible that the pacing cycle length utilized here (500 ms) may have affected the results seen with RSGS on

CV_L and CV_T. Since propagation is related to both cytoplasmic conduction (which is fast and exhibits low resistivity) and GJ conduction (which is relatively slow and exhibits high resistivity), one may expect that the elongated cell geometry would predict how many GJs per unit space the propagating wavefront needs to pass through. Therefore, propagation along the longitudinal axis of the cell travels through fewer junctions per unit space than in transverse and as a result is subject to fewer barriers to conduction (54).

In a Langendorff rabbit heart preparation, Ng et al. (36) indirectly assessed conduction times as the delay between an extra-stimulus impulse (S2) and the beginning of monophasic

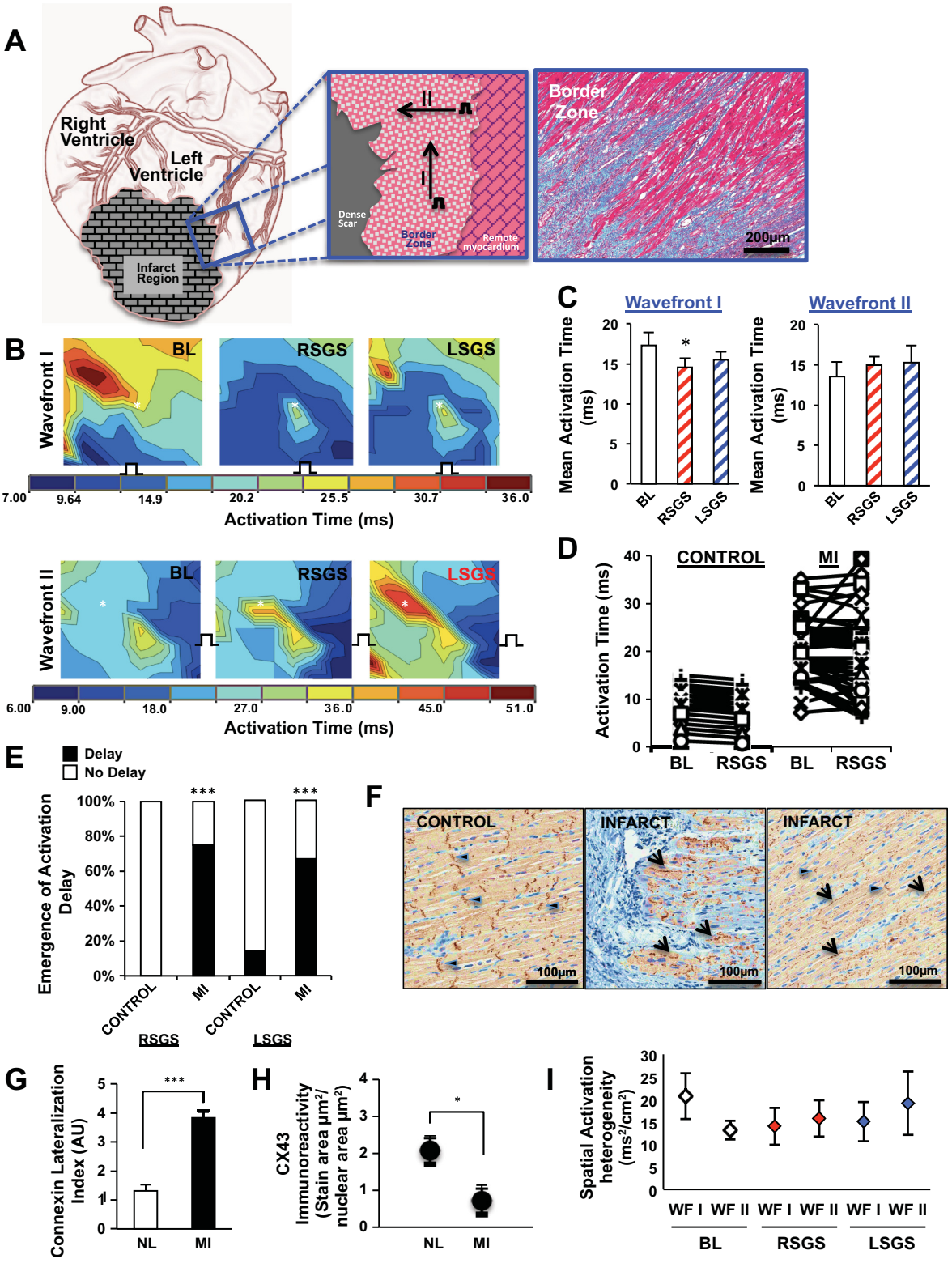

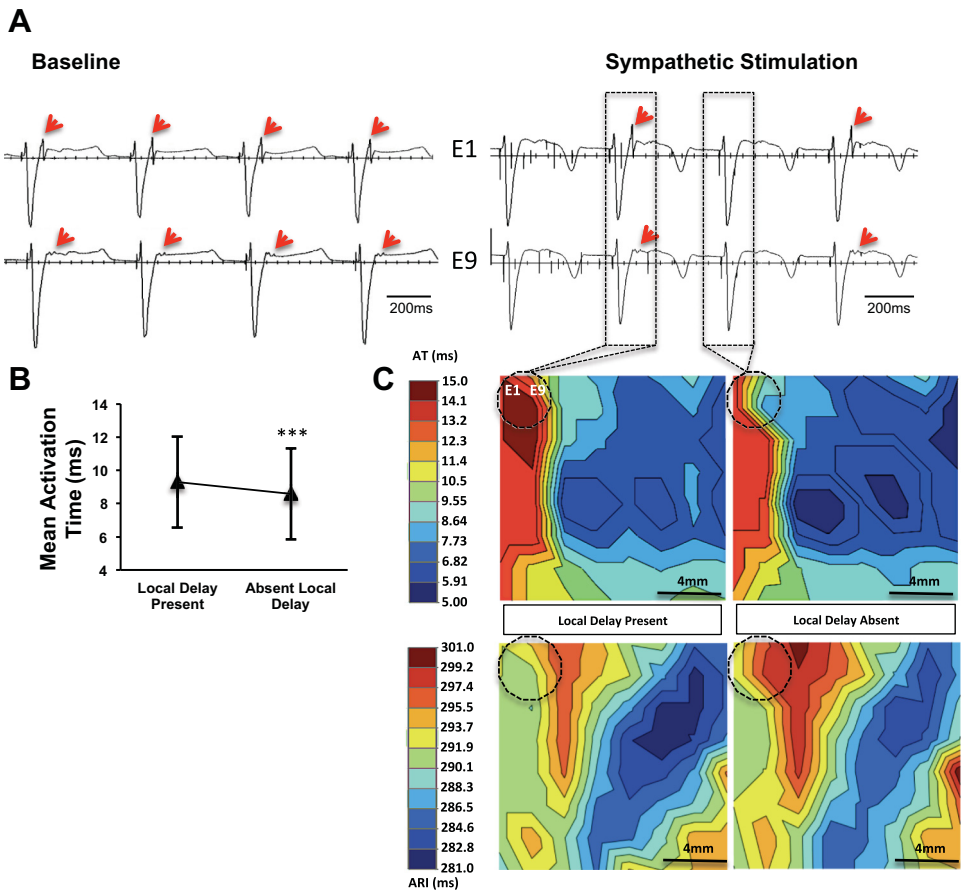

Fig. 7. SGS can alter propagation in putative ventricular tachycardia circuits. *A*: electrograms recorded from the peri-infarct region of a subject, depicting a late potential (LP, red arrows) at baseline and during left sympathetic stimulation. *B*: mean activation time in the region mapped with and without local delay (i.e., LP) (***$P < 0.001$, Student's *t*-test). *C*: propagation (*top row*) and activation recovery interval (*bottom row*) maps with and without local delay (LP). Dashed circle indicated the location of electrodes 1 and 9 (E1 and E9, respectively) recording the LP.

action potential (MAP) signal. In the rabbit preparation, SNS achieved by field stimulation of the outflow aspects of the spinal cord shortened S2-MAP delay by 17%. The direct path taken by the impulse was not measured; hence direct assessment of CV could not be performed, and as such the shortened delay could not be directly ascribed to increased CV. In the present study, the SG were stimulated directly. As such low currents were used with reduced potential of activating other nearby ganglia or nerves with field stimulation (36). Furthermore, the increase in CV observed in our study (20%) is in line with that seen by Ng et al. (17%). The present study represents the first direct demonstration of increased CV by excitation of cardiac sympathetic nerve fibers in an intact neural preparation.

Conduction in peri-infarct zones: impact of sympathoexcitation. The peri-infarct zone between dense scar and surviving myocardium is complex structurally and electrophysiologically, with islands or strands of surviving myocardium surrounded by or interdigitated with scar (33–35). This region is known to harbor structural circuits that maintain monomorphic VT, myocardium exhibiting decreased source-sink mismatch (61), with increased potential for ectopic beats, and increased density of adrenergic nerve endings (9, 58).

We demonstrated that subepicardial fiber orientation remained arranged parallel ("east-west") to the epicardial surface, although there was increased anisotropy just at the edge of the scar. Consistent with previous descriptions (30, 47), we identified decreased Cx-43 density, and extensive lateralization in the peri-infarct zones mapped. CV in this region (as measured by changes in AT) was increased by RSGS in a wavefront-dependent manner. Wavefronts directed superiorly along the scar border demonstrated a significant decrease in AT. Both RSGS and LSGS shortened ARIs in this region (although the effect was smaller with LSGS). These finding highlight two important points: *1*) despite scarring, myocyte loss, and ion channel remodeling, there remains significant functional regu-

Fig. 6. Nonuniform modulation of activation in peri-infarct zones. *A*: illustration of the wavefronts used to assess propagation in the peri-infarct zone is shown at *left* and *middle*, while the fiber arrangement in the a trichrome stain is shown at *right*. *B*: the impact of right and left stellate ganglion stimulation (RSGS and LSGS, respectively) on 2 wavefronts is shown. Not only is the mean activation time decreased in wavefront I, the pattern of propagation is also altered. Wavefront II does not show a decrease in mean AT; however, the impact of SGS on propagation patterns can be appreciated, as well as the emergence of regions of relative or absolute delay (asterisk). *C*: graphical summary of the data for wavefronts I and II are shown. *D*: representative examples of the nonuniformity and paradoxical increases in peri-infarcted vs. control myocardium. *E*: graphical summary of the percentage of animal subjects showing relative or absolute delay in response to SGS. *F*: representative examples of connexin-43 (Cx-43) immunoreacitvity indicating gap junction (GJ) distribution in the regions mapped electrically in control and infarcted animals. Longitudinal (arrowheads) and lateralized (arrows) Cx-43 can be appreciated. Graphical quantifications of Cx-43 lateralization (*G*) and overall density (*H*) are shown ($n = 7$–9, ***$P < 0.001$, *$P < 0.05$, Mann-Whitney test). *I*: spatial activation heterogeneity for wavefronts (WF) I and II at baseline and during RSGS and LSGS.

lation of electrical activation in the peri-infarct zone by cardiac sympathetic nerves, and *2*) there is remodeling of the laterality of sympathetic innervation in the antero-apical region following MI, with increased functional control by LSGS compared with the control state where LSG has little functional effects. This may suggest that growth-associated protein 43 (GAP43)-positive nerve sprouts may arise more from the LSG than RSG in this infarct model (9, 58). It may also reflect structural and functional changes in the LSG or within the intrinsic cardiac network or downregulation of parasympathetic restraining influences (1, 18). Paradoxical increases in AT in the peri-infarct zone may be related to aberrant innervation patterns with preserved parasympathetic but not sympathetic nerve endings, and transdifferentiated neurons to cholinergic phenotype form adrenergic (25). At the level of the myocyte, alterations in ionic properties [e.g., depressed intracellular K^+ and peak calcium transients (39)] and adrenergic signaling pathways [e.g., adrenergic receptor downregulation (28) and decreased G-protein receptor kinase-2 (GRK2) in cardiomyopathy (64)] in surviving peri-infarct myocytes induced by hyperinnervation or local tissue factors may also play a role (16). These findings may underlie the proarrhythmic risk described in association with peri-infarct zone nerve sprouts (9).

Modulation of arrhythmia circuits by peri-infarct innervation. Characteristics of peri-infarct tissue harboring potential circuits within which reentry could occur have been extensively studied and form the basis for catheter ablation studies (23, 24, 51). Although these circuits may exist in many scars, most patients are not incessantly in MMVT. Appropriately timed premature stimuli may modulate the electrical properties of these circuits to initiate MMVT; however, this process is stochastic. As such, functional electrical control of these circuits is critical. In the present study, we present the first direct example of sympathetic nerve modulation of such a circuit in an epicardial peri-infarct zone (Fig. 7, *A*-*C*). In this case, a putative circuit exhibiting a late potential on every depolarization developed functional block during RSGS and permitted conduction on alternating ventricular depolarizations (2:1 conduction pattern). This form of block is prerequisite to make the circuit available for a premature ectopic stimulus propagating slowly within the circuit and, if the conditions are correct, to exit the circuit and capture ventricular myocardium. The well-described decrease in source-sink mismatch in peri-infarct myocardium increases the likelihood that such stimuli result in ventricular capture (39).

Functional modulation of such circuits likely occurs on a dynamic basis in vivo, depending on the sympathetic state of the subject. Parasympathetic neurotransmission, known to be present at all levels of sympathetic tone, likely plays a significant role in neurotransmission (45). During exercise, stress, general anesthesia, and sleep, for example, neurotransmission (both sympathetic and parasympathetic) likely modulates the electrophysiologic properties of peri-infarct circuits capable of harboring VT. Therapeutic modulation may be achieved by sympathectomy, vagal stimulation, tragal stimulation, and/or spinal cord stimulation (3, 45). These interventions warrant study on how peri-infarct circuits are modulated.

Limitations. In this study, we mapped an equivalent region of the antero-apical epicardium in normal and infarcted hearts. Whether other regions of the peri-infarct zone (for example, right ventricular apex or posterior LV) exhibit similar findings is unclear. Furthermore, remodeling of sympathetic nerves and neurons has been described, and the roles of other neurotransmitters such as neuropeptide Y were not explored. In addition, whether sympathoexcitation-mediated changes in the peri-infarct zone are prevented by β-blockade was not studied. While there is agreement on the use of local EGMs to estimate local activation (8), the use of the activation recovery interval to

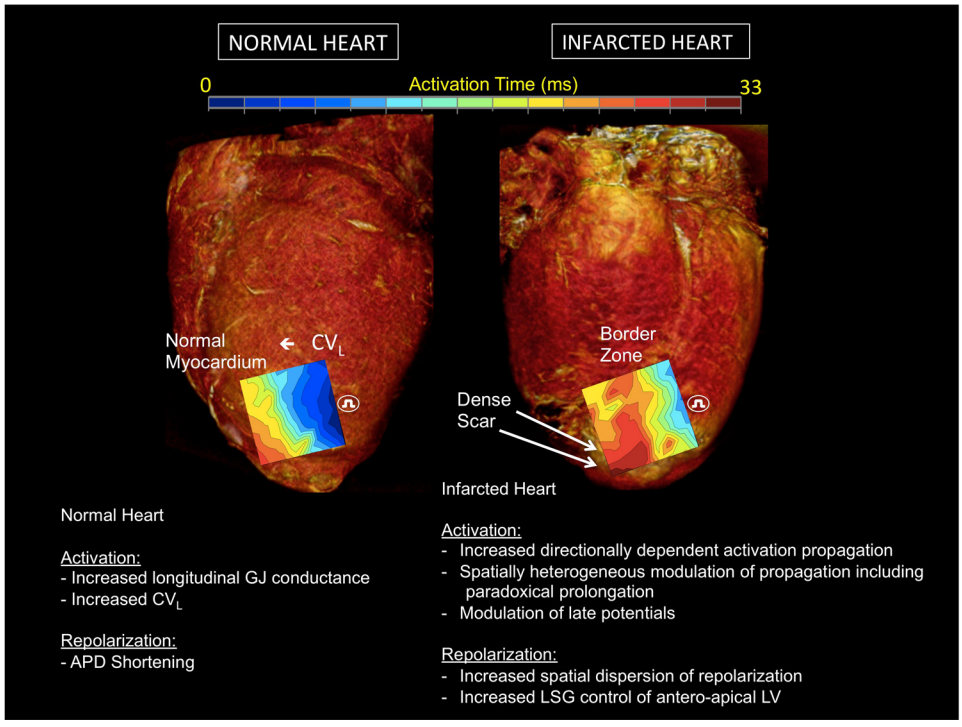

Fig. 8. Cardiac electrical indices during sympathoexcitation in normal and infarcted hearts. A schematic figure illustrating the effects of sympathetic activation on myocardial activation and repolarization in normal hearts, and in the peri-infarcted region of animals with ischemic cardiomyopathy. APD, action potential duration; β, beta; CV_L, longitudinal conduction velocity; CV_T, transverse conduction velocity; GJ, gap junction; LSG, left stellate ganglion; LV, left ventricle. CV anisotropy = CV_L/CV_T. Impact of β-adrenergic receptor activation on GJ conductance from de Boer et al. (13).

estimate local APD has limitations. The orientation of the T wave (positive vs. negative) may result in error in estimation of the local APD (12). The model used in this study, with its intact neural connections and preservation of neural reflexes by the anesthetic regimen, has improved the sensitivity of detecting electrical perturbations by sympathoexcitation. Although no arrhythmias were induced for this work, the arrhythmogenic implications of these findings are significant.

Conclusions. Taken together, the data presented herein for the first time, demonstrate the impact of excitation of sympathetic fibers innervating the heart on electrical propagation in normal and infarcted hearts. These data highlight the important role adrenergic activation plays in altering propagation patterns (Fig. 8), with the critical potential of initiating and maintaining ventricular arrhythmias. The data also emphasize the dynamic nature of the peri-infarct substrate and its functional modulation by sympathetic innervation, emphasizing the critical role the autonomic nervous system plays in arrhythmogenesis.

ACKNOWLEDGMENTS

We thank Amiksha Gandhi, Dr. Tatsuo Takamiya, and Dr. Keijiro Nakamura for excellent technical assistance.

GRANTS

This study was supported by National Heart, Lung, and Blood Institute Grants HL-125730 (to O. A. Ajijola) and HL-084261 (to K. Shivkumar) and in part by software from the National Institute of General Medical Sciences Center for Integrative Biomedical Computing (2P41RR0112553-2; University of Utah).

DISCLOSURES

No conflicts of interest, financial or otherwise, are declared by the author(s).

AUTHOR CONTRIBUTIONS

O.A.A. conceived and designed research; O.A.A., A.K., O.K., and E.A. performed experiments; O.A.A., A.K., O.K., E.A., D.E., and M.C.F. analyzed data; O.A.A., R.L.L., E.A., D.E., M.C.F., J.L.A., and K.S. interpreted results of experiments; O.A.A. and M.C.F. prepared figures; O.A.A. drafted manuscript; O.A.A., R.L.L., A.K., O.K., E.A., D.E., M.C.F., J.L.A., and K.S. edited and revised manuscript; O.A.A., R.L.L., A.K., O.K., E.A., D.E., M.C.F., J.L.A., and K.S. approved final version of manuscript.

REFERENCES

1. **Ajijola OA, Wisco JJ, Lambert HW, Mahajan A, Stark E, Fishbein MC, Shivkumar K.** Extracardiac neural remodeling in humans with cardiomyopathy. *Circ Arrhythm Electrophysiol* 5: 1010–1116, 2012. doi:10.1161/CIRCEP.112.972836.
2. **Ajijola OA, Yagishita D, Patel KJ, Vaseghi M, Zhou W, Yamakawa K, So E, Lux RL, Mahajan A, Shivkumar K.** Focal myocardial infarction induces global remodeling of cardiac sympathetic innervation: neural remodeling in a spatial context. *Am J Physiol Heart Circ Physiol* 305: H1031–H1040, 2013. doi:10.1152/ajpheart.00434.2013.
3. **Ardell JL, Andresen MC, Armour JA, Billman GE, Chen PS, Foreman RD, Herring N, O'Leary DS, Sabbah HN, Schultz HD, Sunagawa K, Zucker IH.** Translational neurocardiology: preclinical models and cardioneural integrative aspects. *J Physiol* 594: 3877–3909, 2016. doi:10.1113/JP271869.
4. **Atkinson A, Inada S, Li J, Tellez JO, Yanni J, Sleiman R, Allah EA, Anderson RH, Zhang H, Boyett MR, Dobrzynski H.** Anatomical and molecular mapping of the left and right ventricular His-Purkinje conduction networks. *J Mol Cell Cardiol* 51: 689–701, 2011. doi:10.1016/j.yjmcc.2011.05.020.
5. **Ben-David J, Zipes DP.** Differential response to right and left ansae subclaviae stimulation of early afterdepolarizations and ventricular tachycardia induced by cesium in dogs. *Circulation* 78: 1241–1250, 1988. doi:10.1161/01.CIR.78.5.1241.
6. **Bers DM.** *Excitation-Contraction Coupling and Cardiac Contractile Force*. Dordrecht, The Netherlands: Kluwer, 2001, p. xxiv. doi:10.1007/978-94-010-0658-3.
7. **Campbell AS, Johnstone SR, Baillie GS, Smith G.** β-Adrenergic modulation of myocardial conduction velocity: connexins vs. sodium current. *J Mol Cell Cardiol* 77: 147–154, 2014. doi:10.1016/j.yjmcc.2014.09.030.
8. **Cantwell CD, Roney CH, Ng FS, Siggers JH, Sherwin SJ, Peters NS.** Techniques for automated local activation time annotation and conduction velocity estimation in cardiac mapping. *Comput Biol Med* 65: 229–242, 2015. doi:10.1016/j.compbiomed.2015.04.027.
9. **Cao JM, Fishbein MC, Han JB, Lai WW, Lai AC, Wu TJ, Czer L, Wolf PL, Denton TA, Shintaku IP, Chen PS, Chen LS.** Relationship between regional cardiac hyperinnervation and ventricular arrhythmia. *Circulation* 101: 1960–1969, 2000. doi:10.1161/01.CIR.101.16.1960.
10. **Clerc L.** Directional differences of impulse spread in trabecular muscle from mammalian heart. *J Physiol* 255: 335–346, 1976. doi:10.1113/jphysiol.1976.sp011283.
11. **Conrath CE, Opthof T.** Ventricular repolarization: an overview of (patho)physiology, sympathetic effects and genetic aspects. *Prog Biophys Mol Biol* 92: 269–307, 2006. doi:10.1016/j.pbiomolbio.2005.05.009.
12. **Coronel R, de Bakker JM, Wilms-Schopman FJ, Opthof T, Linnenbank AC, Belterman CN, Janse MJ.** Monophasic action potentials and activation recovery intervals as measures of ventricular action potential duration: experimental evidence to resolve some controversies. *Heart Rhythm* 3: 1043–1050, 2006. doi:10.1016/j.hrthm.2006.05.027.
13. **de Boer TP, van Rijen HV, Van der Heyden MA, Kok B, Opthof T, Vos MA, Jongsma HJ, de Bakker JM, van Veen TA.** Beta-, not alpha-adrenergic stimulation enhances conduction velocity in cultures of neonatal cardiomyocytes. *Circ J* 71: 973–981, 2007. doi:10.1253/circj.71.973.
14. **de Groot JR, Veenstra T, Verkerk AO, Wilders R, Smits JP, Wilms-Schopman FJ, Wiegerinck RF, Bourier J, Belterman CN, Coronel R, Verheijck EE.** Conduction slowing by the gap junctional uncoupler carbenoxolone. *Cardiovasc Res* 60: 288–297, 2003. doi:10.1016/j.cardiores.2003.07.004.
15. **Draper MH, Mya-Tu M.** A comparison of the conduction velocity in cardiac tissues of various mammals. *Q J Exp Physiol Cogn Med Sci* 44: 91–109, 1959.
16. **Gardner RT, Ripplinger CM, Myles RC, Habecker BA.** Molecular mechanisms of sympathetic remodeling and arrhythmias. *Circ Arrhythm Electrophysiol* 9: e001359, 2016. doi:10.1161/CIRCEP.115.001359.
17. **Giepmans BN.** Gap junctions and connexin-interacting proteins. *Cardiovasc Res* 62: 233–245, 2004. doi:10.1016/j.cardiores.2003.12.009.
18. **Hardwick JC, Southerland EM, Ardell JL.** Chronic myocardial infarction induces phenotypic and functional remodeling in the guinea pig cardiac plexus. *Am J Physiol Regul Integr Comp Physiol* 295: R1926–R1933, 2008. doi:10.1152/ajpregu.90306.2008.
19. **Haws CW, Lux RL.** Correlation between in vivo transmembrane action potential durations and activation-recovery intervals from electrograms. Effects of interventions that alter repolarization time. *Circulation* 81: 281–288, 1990. doi:10.1161/01.CIR.81.1.281.
20. **Heemskerk AM, Damon BM.** Diffusion tensor MRI assessment of skeletal muscle architecture. *Curr Med Imaging Rev* 3: 152–160, 2007. doi:10.2174/157340507781386988.
21. **Hélie F, Vinet A, Cardinal R.** Spatiotemporal dynamics of reentrant ventricular tachycardias in canine myocardial infarction: pharmacological modulation. *Can J Physiol Pharmacol* 81: 413–422, 2003. doi:10.1139/y03-040.
22. **Jongsma HJ, Wilders R.** Gap junctions in cardiovascular disease. *Circ Res* 86: 1193–1197, 2000. doi:10.1161/01.RES.86.12.1193.
23. **Josephson ME, Horowitz LN, Farshidi A.** Continuous local electrical activity. A mechanism of recurrent ventricular tachycardia. *Circulation* 57: 659–665, 1978. doi:10.1161/01.CIR.57.4.659.
24. **Josephson ME, Simson MB, Harken AH, Horowitz LN, Falcone RA.** The incidence and clinical significance of epicardial late potentials in patients with recurrent sustained ventricular tachycardia and coronary artery disease. *Circulation* 66: 1199–1204, 1982. doi:10.1161/01.CIR.66.6.1199.
25. **Kanazawa H, Ieda M, Kimura K, Arai T, Kawaguchi-Manabe H, Matsuhashi T, Endo J, Sano M, Kawakami T, Kimura T, Monkawa T, Hayashi M, Iwanami A, Okano H, Okada Y, Ishibashi-Ueda H, Ogawa S, Fukuda K.** Heart failure causes cholinergic transdifferentiation

of cardiac sympathetic nerves via gp130-signaling cytokines in rodents. *J Clin Invest* 120: 408–421, 2010. doi:10.1172/JCI39778.

26. **Kojodjojo P, Kanagaratnam P, Segal OR, Hussain W, Peters NS.** The effects of carbenoxolone on human myocardial conduction: a tool to investigate the role of gap junctional uncoupling in human arrhythmogenesis. *J Am Coll Cardiol* 48: 1242–1249, 2006. doi:10.1016/j.jacc.2006.04.093.
27. **Kralios FA, Martin L, Burgess MJ, Millar K.** Local ventricular repolarization changes due to sympathetic nerve-branch stimulation. *Am J Physiol* 228: 1621–1626, 1975.
28. **Lefkowitz RJ, Rockman HA, Koch WJ.** Catecholamines, cardiac beta-adrenergic receptors, and heart failure. *Circulation* 101: 1634–1637, 2000. doi:10.1161/01.CIR.101.14.1634.
29. **Lu T, Lee HC, Kabat JA, Shibata EF.** Modulation of rat cardiac sodium channel by the stimulatory G protein alpha subunit. *J Physiol* 518: 371–384, 1999. doi:10.1111/j.1469-7793.1999.0371p.x.
30. **Macia E, Dolmatova E, Cabo C, Sosinsky AZ, Dun W, Coromilas J, Ciaccio EJ, Boyden PA, Wit AL, Duffy HS.** Characterization of gap junction remodeling in epicardial border zone of healing canine infarcts and electrophysiological effects of partial reversal by rotigaptide. *Circ Arrhythm Electrophysiol* 4: 344–351, 2011. doi:10.1161/CIRCEP.110.959312.
31. **Matsuda JJ, Lee H, Shibata EF.** Enhancement of rabbit cardiac sodium channels by beta-adrenergic stimulation. *Circ Res* 70: 199–207, 1992. doi:10.1161/01.RES.70.1.199.
32. **Millar CK, Kralios FA, Lux RL.** Correlation between refractory periods and activation-recovery intervals from electrograms: effects of rate and adrenergic interventions. *Circulation* 72: 1372–1379, 1985. doi:10.1161/01.CIR.72.6.1372.
33. **Nakahara S, Tung R, Ramirez RJ, Gima J, Wiener I, Mahajan A, Boyle NG, Shivkumar K.** Distribution of late potentials within infarct scars assessed by ultra high-density mapping. *Heart Rhythm* 7: 1817–1824, 2010. doi:10.1016/j.hrthm.2010.07.032.
34. **Nakahara S, Tung R, Ramirez RJ, Michowitz Y, Vaseghi M, Buch E, Gima J, Wiener I, Mahajan A, Boyle NG, Shivkumar K.** Characterization of the arrhythmogenic substrate in ischemic and nonischemic cardiomyopathy implications for catheter ablation of hemodynamically unstable ventricular tachycardia. *J Am Coll Cardiol* 55: 2355–2365, 2010. doi:10.1016/j.jacc.2010.01.041.
35. **Nakahara S, Vaseghi M, Ramirez RJ, Fonseca CG, Lai CK, Finn JP, Mahajan A, Boyle NG, Shivkumar K.** Characterization of myocardial scars: electrophysiological imaging correlates in a porcine infarct model. *Heart Rhythm* 8: 1060–1067, 2011. doi:10.1016/j.hrthm.2011.02.029.
36. **Ng GA, Brack KE, Patel VH, Coote JH.** Autonomic modulation of electrical restitution, alternans and ventricular fibrillation initiation in the isolated heart. *Cardiovasc Res* 73: 750–760, 2007. doi:10.1016/j.cardiores.2006.12.001.
37. **Nguyen C, Fan Z, Xie Y, Dawkins J, Tseliou E, Bi X, Sharif B, Dharmakumar R, Marbán E, Li D.** In vivo contrast free chronic myocardial infarction characterization using diffusion-weighted cardiovascular magnetic resonance. *J Cardiovasc Magn Reson* 16: 68, 2014. doi:10.1186/s12968-014-0068-y.
38. **Opthof T, Misier AR, Coronel R, Vermeulen JT, Verberne HJ, Frank RG, Moulijn AC, van Capelle FJ, Janse MJ.** Dispersion of refractoriness in canine ventricular myocardium. Effects of sympathetic stimulation. *Circ Res* 68: 1204–1215, 1991.
39. **Pinto JM, Boyden PA.** Electrical remodeling in ischemia and infarction. *Cardiovasc Res* 42: 284–297, 1999. doi:10.1016/S0008-6363(99)00013-9.
40. **Pop M, Ghugre NR, Ramanan V, Morikawa L, Stanisz G, Dick AJ, Wright GA.** Quantification of fibrosis in infarcted swine hearts by ex vivo late gadolinium-enhancement and diffusion-weighted MRI methods. *Phys Med Biol* 58: 5009–5028, 2013. doi:10.1088/0031-9155/58/15/5009.
41. **Rajendran PS, Nakamura K, Ajijola OA, Vaseghi M, Armour JA, Ardell JL, Shivkumar K.** Myocardial infarction induces structural and functional remodeling of the intrinsic cardiac nervous system. *J Physiol* 594: 321–341, 2015. doi:10.1113/JP271165.
42. **Ramirez RJ, Ajijola OA, Zhou W, Holmström B, Lüning H, Laks MM, Shivkumar K, Mahajan A.** A new electrocardiographic marker for sympathetic nerve stimulation: modulation of repolarization by stimulation of stellate ganglia. *J Electrocardiol* 44: 694–699, 2011. doi:10.1016/j.jelectrocard.2011.07.030.
43. **Salameh A, Dhein S.** Adrenergic control of cardiac gap junction function and expression. *Naunyn Schmiedebergs Arch Pharmacol* 383: 331–346, 2011. doi:10.1007/s00210-011-0603-4.
44. **Sano T, Takayama N, Shimamoto T.** Directional difference of conduction velocity in the cardiac ventricular syncytium studied by microelectrodes. *Circ Res* 7: 262–267, 1959. doi:10.1161/01.RES.7.2.262.
45. **Shivkumar K, Ajijola OA, Anand I, Armour JA, Chen PS, Esler M, De Ferrari GM, Fishbein MC, Goldberger JJ, Harper RM, Joyner MJ, Khalsa SS, Kumar R, Lane R, Mahajan A, Po S, Schwartz PJ, Somers VK, Valderrabano M, Vaseghi M, Zipes DP.** Clinical neurocardiology defining the value of neuroscience-based cardiovascular therapeutics. *J Physiol* 594: 3911–3954, 2016. doi:10.1113/JP271870.
46. **Smaill BH, Zhao J, Trew ML.** Three-dimensional impulse propagation in myocardium: arrhythmogenic mechanisms at the tissue level. *Circ Res* 112: 834–848, 2013. doi:10.1161/CIRCRESAHA.111.300157.
47. **Smith JH, Green CR, Peters NS, Rothery S, Severs NJ.** Altered patterns of gap junction distribution in ischemic heart disease. An immunohistochemical study of human myocardium using laser scanning confocal microscopy. *Am J Pathol* 139: 801–821, 1991.
48. **Spach MS, Dolber PC.** Relating extracellular potentials and their derivatives to anisotropic propagation at a microscopic level in human cardiac muscle. Evidence for electrical uncoupling of side-to-side fiber connections with increasing age. *Circ Res* 58: 356–371, 1986. doi:10.1161/01.RES.58.3.356.
49. **Spach MS, Kootsey JM, Sloan JD.** Active modulation of electrical coupling between cardiac cells of the dog. A mechanism for transient and steady state variations in conduction velocity. *Circ Res* 51: 347–362, 1982. doi:10.1161/01.RES.51.3.347.
50. **Stankovicová T, Bito V, Heinzel F, Mubagwa K, Sipido KR.** Isolation and morphology of single Purkinje cells from the porcine heart. *Gen Physiol Biophys* 22: 329–340, 2003.
51. **Stevenson WG, Friedman PL, Sager PT, Saxon LA, Kocovic D, Harada T, Wiener I, Khan H.** Exploring postinfarction reentrant ventricular tachycardia with entrainment mapping. *J Am Coll Cardiol* 29: 1180–1189, 1997. doi:10.1016/S0735-1097(97)00065-X.
52. **Streeter DD, Bassett DL.** An engineering analysis of myocardial fiber orientation in pigs left ventricle in systole. *Anat Rec* 155: 503–511, 1966. doi:10.1002/ar.1091550403.
53. **Ueda H, Yanai Y, Murao S, Harumi K, Mashima S, Kuroiwa A, Sugimoto T, Shimomura D.** Electrocardiographic and vectorcardiographic changes produced by electrical stimulation of the cardiac nerves. *Jpn Heart J* 5: 359–372, 1964. doi:10.1536/ihj.5.359.
54. **Valderrábano M.** Influence of anisotropic conduction properties in the propagation of the cardiac action potential. *Prog Biophys Mol Biol* 94: 144–168, 2007. doi:10.1016/j.pbiomolbio.2007.03.014.
55. **Vaseghi M, Gima J, Kanaan C, Ajijola OA, Marmureanu A, Mahajan A, Shivkumar K.** Cardiac sympathetic denervation in patients with refractory ventricular arrhythmias or electrical storm: intermediate and long-term follow-up. *Heart Rhythm* 11: 360–366, 2014. doi:10.1016/j.hrthm.2013.11.028.
56. **Vaseghi M, Lux RL, Mahajan A, Shivkumar K.** Sympathetic stimulation increases dispersion of repolarization in humans with myocardial infarction. *Am J Physiol Heart Circ Physiol* 302: H1838–H1846, 2012. doi:10.1152/ajpheart.01106.2011.
57. **Vaseghi M, Yamakawa K, Sinha A, So EL, Zhou W, Ajijola OA, Lux RL, Laks M, Shivkumar K, Mahajan A.** Modulation of regional dispersion of repolarization and T-peak to T-end interval by the right and left stellate ganglia. *Am J Physiol Heart Circ Physiol* 305: H1020–H1030, 2013. doi:10.1152/ajpheart.00056.2013.
58. **Vracko R, Thorning D, Frederickson RG.** Nerve fibers in human myocardial scars. *Hum Pathol* 22: 138–146, 1991. doi:10.1016/0046-8177(91)90035-N.
59. **Wallace AG, Sarnoff SJ.** Effects of cardiac sympathetic nerve stimulation on conduction in the heart. *Circ Res* 14: 86–92, 1964. doi:10.1161/01.RES.14.1.86.
60. **Weidmann S.** Electrical constants of trabecular muscle from mammalian heart. *J Physiol* 210: 1041–1054, 1970. doi:10.1113/jphysiol.1970.sp009256.
61. **Xie Y, Sato D, Garfinkel A, Qu Z, Weiss JN.** So little source, so much sink: requirements for afterdepolarizations to propagate in tissue. *Biophys J* 99: 1408–1415, 2010. doi:10.1016/j.bpj.2010.06.042.
62. **Yancy CW, Jessup M, Bozkurt B, Butler J, Casey DE Jr, Drazner MH, Fonarow GC, Geraci SA, Horwich T, Januzzi JL, Johnson MR, Kasper EK, Levy WC, Masoudi FA, McBride PE, McMurray JJ, Mitchell JE, Peterson PN, Riegel B, Sam F, Stevenson LW, Tang WH, Tsai EJ, Wilkoff BL; American College of Cardiology**

Foundation; American Heart Association Task Force on Practice Guidelines. 2013 ACCF/AHA guideline for the management of heart failure: a report of the American College of Cardiology Foundation/American Heart Association Task Force on Practice Guidelines. *J Am Coll Cardiol* 62: e147–e239, 2013. doi:10.1016/j.jacc.2013.05.019.

63. **Yanowitz F, Preston JB, Abildskov JA.** Functional distribution of right and left stellate innervation to the ventricles. Production of neurogenic electrocardiographic changes by unilateral alteration of sympathetic tone. *Circ Res* 18: 416–428, 1966. doi:10.1161/01.RES.18.4.416.
64. **Yatani A, Shen YT, Yan L, Chen W, Kim SJ, Sano K, Irie K, Vatner SF, Vatner DE.** Down regulation of the L-type Ca^{2+} channel, GRK2, and phosphorylated phospholamban: protective mechanisms for the denervated failing heart. *J Mol Cell Cardiol* 40: 619–628, 2006. doi:10.1016/j.yjmcc.2006.02.002.